PERGAMON

Journal of Structural Geology 23 (2001) 1825–1844

JOURNAL OF STRUCTURAL GEOLOGY

www.elsevier.com/locate/jstrugeo

Damage zone and slip-surface evolution over μm to km scales in high-porosity Navajo sandstone, Utah

Z.K. Shipton*, P.A. Cowie

Department of Geology & Geophysics, Edinburgh University, West Mains Road, Edinburgh, EH9 3JW, UK

Received 1 September 2000; revised 1 March 2001; accepted 6 March 2001

Abstract

Detailed mapping of throw variations and deformation along two km-scale normal faults in the high-porosity Navajo sandstone, Utah, has been used to investigate fault growth in this lithology. The faults consist of one or more through-going, striated, slip-surfaces, accommodating the greater part of the offset surrounded by a damage zone consisting of deformation band clusters and short, unconnected slip-surfaces. In contrast to previous models for deformation in this lithology, we find that the nucleation of slip-surfaces begins where measurable throw is negligible and deformation bands are forming and increasing in number. The microstructure and porosity of deformation bands and slip surfaces are distinct and independent of the amount of offset that they accommodate, i.e. they represent different and yet contemporaneous deformation mechanisms. The point where measurable throw begins to accumulate (the fault tip) is marked by the first through-going connected slip-surface. Increase in throw towards the centre of the fault results in a three-dimensional strain field, producing orthorhombic structural geometries within the damage zone. We find that the total width of the damage zone increases as offset is accumulated. For these faults, the damage zone width is approximately 2.5 times the total fault throw.

1. Introduction

Fault zones commonly consist of a fault core in which the greater part of the displacement is accommodated, surrounded by a zone of deformation referred to as the damage zone (Chester and Logan, 1986). Damage zone deformation can be a result of fault rupture events, propagation of the fault tip, or flexure of the rock in the volume around a fault to accommodate offset. A fault zone must therefore be considered as a four-dimensional system consisting of slip along the main fault surface and deformation within a volume around that surface, accumulating strain through time. The time dimension is usually the most difficult to constrain, although cross-cutting relationships may give an indication of relative timing.

Many published studies of fault zone architecture take the form of maps or two-dimensional geometrical descriptions of fault geometry without any explicit consideration of temporal evolution (e.g. Brock and Engelder, 1977; Jamison and Stearns, 1982; Chester and Logan, 1986; Chester et al., 1993; Antonellini and Aydin, 1995; McGrath and Davison, 1995; Little, 1996; Foxford et al., 1998; Martel and Boger, 1998; Schulz and Evans, 1998). Three-dimensional seismic data may give an indication of fault zone structure in the third dimension, but the finite resolution of the data always poses a severe limitation on interpretation (e.g. Mansfield and Cartwright, 1996; Knott et al., 1996). In any case, these maps are only snapshots of the fault's evolution in time. Rock deformation experiments allow the evolution of structures through time to be investigated (e.g. Cox and Scholz, 1988; Lockner et al., 1992; Mair et al., 2000), but are limited in the time and length scales that they can represent.

One way to infer the temporal evolution is by comparing faults that have different amounts of displacement, the idea being that faults with small displacements represent the early stages of development of a larger fault. This approach may be used to document how the damage zone varies in width and structural complexity as a fault grows. For example, Antonellini and Aydin (1994) and Aydin and Johnson (1978) developed a model for fault zone development in high-porosity sandstones in this way. However, to produce their model they compared different faults that had different amounts of displacement. Other workers have taken a similar approach but for faults that are not in precisely the same lithology, e.g., combining data on faults within a stratigraphic section that consists of petrographically

* Corresponding author. Now at: Department of Geology, Utah State University, 4505 Old Main Hill, Logan, UT 84322, USA.
E-mail address: zshipton@cc.usu.edu (Z.K. Shipton).

0191-8141/01/$ - see front matter
PII: S0191-8141(01)00035-9

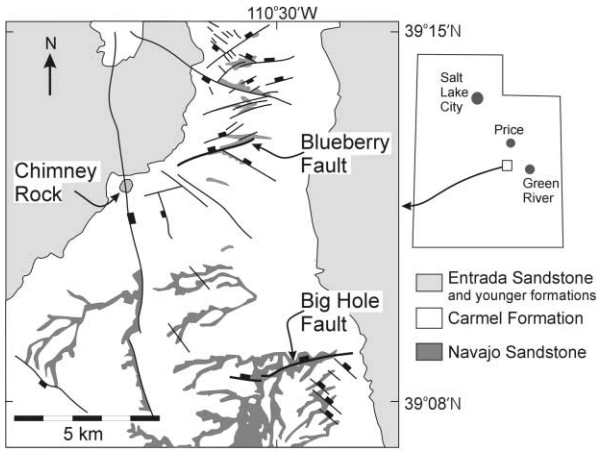

Fig. 1. Map of the Chimney Rock fault array showing the location of the faults in this study (after Witkind, 1988). Ticks mark the downthrown side of the faults.

distinct units (e.g. Knott et al., 1996). Vermilye and Scholz (1998) examined fault zone architecture along strike of individual metre-scale faults but displacement along these faults is not well constrained. The present study is unique in that we have examined the three-dimensional architecture of individual faults, in the same lithology (high-porosity sandstone), as a function of measured displacement along strike from the fault tips where the displacement is negligible to the fault centre where the displacement is tens of metres. Furthermore, exposures beyond the point of measurable displacement (i.e., beyond the tip) allow us to document the nature of the process zone in this lithology.

Deformation of weakly cemented, high-porosity (>10%) sandstone characteristically results in the formation of deformation bands. These are thin anastomosing bands of cataclasis (<5 mm thick), each with a few millimetres offset (Dunn et al., 1973; Aydin, 1978; Aydin and Johnson, 1978; Pittman, 1981). On average the offset across a zone of deformation bands is proportional to the number of bands in the zone (Aydin and Johnson, 1978; Mair et al., 2000). Narrow (<1 mm thick), planar, polished, slip-surfaces occur within and along the edges of clusters of deformation bands. Unlike deformation band zones, slip-surfaces can accumulate very large offsets (metres to hundreds of metres). Although the process of deformation band growth has been described in detail (Aydin and Johnson, 1978, 1983; Antonellini and Aydin, 1994), little attention has been paid to the transition from the addition of deformation bands to a zone, to the accumulation of substantial offset on a slip-surface. Deformation bands have been shown to be effective hydrocarbon and water seals even at very small offsets (Antonellini and Aydin, 1999; Edwards et al., 1993). If slip-surfaces remain as open fractures at depth, they may present an enhanced permeability within a damage zone that otherwise may have very low permeability (Antonellini and Aydin, 1994; Shipton et al., 2001, in press). Consequently, understanding the evolution of slip-surfaces within networks of deformation bands is crucial for the prediction of fault zone permeability.

In this paper we present structural data related to along-strike throw variations on two km-scale normal faults in the Jurassic Navajo Sandstone, Utah, USA. We have characterised the structural style at the outcrop-scale as well as at the grain-scale, via systematic sampling, and linked this to well-constrained throw measurements. Outcrop-scale maps are presented, first at the fault tip where the throw ranges from zero to 4 m, and then at increasing throws of 8, 17, and 20 m. Microstructural analysis of samples taken at increasing values of throw are linked to the macroscopic features. By integrating these observations, and including an analysis of porosity structure, we build up a picture of how the damage zone around these faults evolved as throw accumulated. We show conclusively that the observed structures cannot be explained without considering fault growth processes, i.e. lateral propagation and accumulation of offset. Furthermore, we discuss the formation of slip surfaces and how they relate to deformation band development and the formation of large offset faults in this lithology.

2. Geological setting

The Chimney Rock Fault array (Fig. 1) consists of normal faults ranging from 100 m to 6 km in length. The faults are steeply dipping (70–80°), gently undulating surfaces with predominantly dip-slip slickenside lineations. The origin of the faults is uncertain, but it is likely that they formed in response to the uplift of the Laramide age (50 Ma) San Rafael Swell (Shipton, 1999): a north–south trending fold above a reactivated basement reverse fault. If this is the case then the faults formed at between 1.5 and 3.0 km depth, the likely amount of overburden in the region at 50 Ma (i.e. a maximum temperature of the order of 100°C and pressure of 80 MPa).

There are four mutually cross-cutting (synchronous) fault sets in the Chimney Rock Fault array: two strike sets, each with two dip directions (Fig. 1). The two faults in this study trend ENE–WSW and dip to the north. The other strike set in the region trends ESE–WNW. This type of orthorhombic fault geometry has been interpreted as the result of growth in a three-dimensional strain field (Reches, 1978, 1983; Aydin and Reches, 1982; Krantz, 1988a, 1989). In this case, the Chimney Rock Faults have developed in response to a maximum extensional strain axis oriented north–south, a minimum extensional strain axis oriented east–west, and a vertical compressive strain axis (Krantz, 1988a).

Two faults were selected for detailed study. The Blueberry Fault is 3.6 km long with a maximum throw of 30 m. The eastern tip of this fault is superbly exposed in a dry river canyon and detailed measurements of the throw profile at the fault tip are presented in Cowie and Shipton (1998). The 4.1 km long Big Hole Fault is also exposed in a deeply incised canyon and has a maximum throw of 29 m. This fault has not previously been mapped in detail, but does

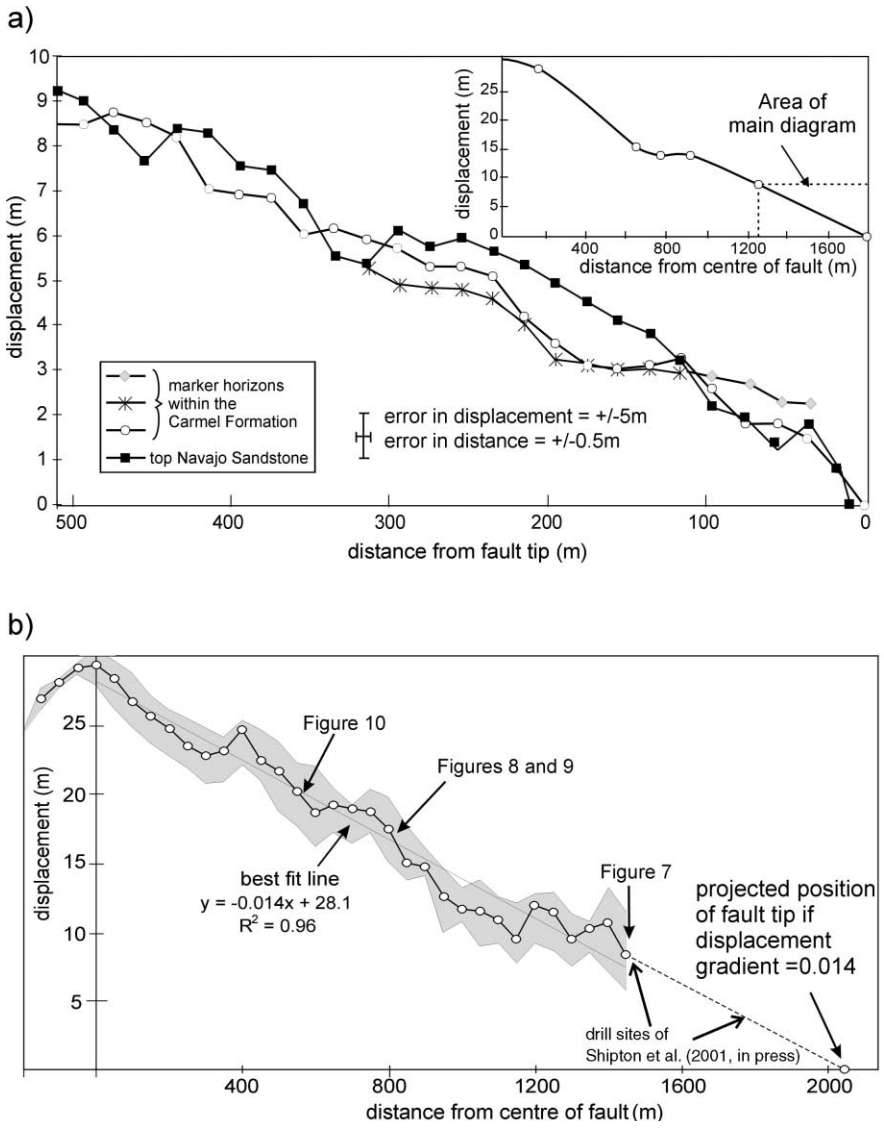

Fig. 2. (a) Displacement profile for the Blueberry Fault tip (from Cowie and Shipton, 1998). Displacement was measured on four marker horizons within the Carmel Formation. The inset shows measured points for the eastern half of the fault from Krantz (1988a). (b) Displacement profile for the eastern end of the Big Hole fault. One horizon within the Carmel Formation was surveyed in this area. The eastern tip of the fault is buried under Quaternary deposits, so the position of the tip is inferred using the best-fit displacement gradient (close to that at the Blueberry Fault tip). The grey area represents the error due to variation in bedding strike.

appear on the USGS 1:250,000 geological map (Witkind, 1988). The eastern end of the Big Hole Fault does not appear to link with any other faults along strike and has a symmetrical throw profile characteristic of isolated faults (e.g. Dawers and Anders, 1995; Nicol et al., 1996). It can therefore be thought of as approximating an ideal, radially propagating fault. The eastern tip of the Big Hole Fault is buried beneath Quaternary sediments, however because the two faults are of similar size, we treat the Blueberry Fault tip as a proxy for the tip of the Big Hole Fault.

The faults cut the aeolian Navajo Sandstone. This is a planar to cross-bedded, fine to medium-grained, well-sorted, well-rounded sandstone with ~90–95% quartz, 1–6% feldspar, and 1–3% clays, and an average porosity of 20% (Dunn et al., 1973). In our study area it contains a minor amount of syntaxial quartz overgrowths with occasional calcite cement and is stained with hematite, giving it a honey-brown colour. The Navajo Sandstone in the study area is 137–151 m thick. It overlies the Triassic Kayenta Formation, a 30–80 m thick siltstone and sandstone, and the Wingate Sandstone, a 100–120 m thick aeolian sandstone. Observations of fault spacing (Krantz, 1988b), suggest that the Chimney Rock Faults are mostly confined to within the Navajo Sandstone. The Navajo Sandstone is overlain by the thinly bedded marine marls and limestones of the Carmel Formation, which provide ideal marker horizons for measuring throw. We focus here on the development of damage zone structures only in the Navajo Sandstone.

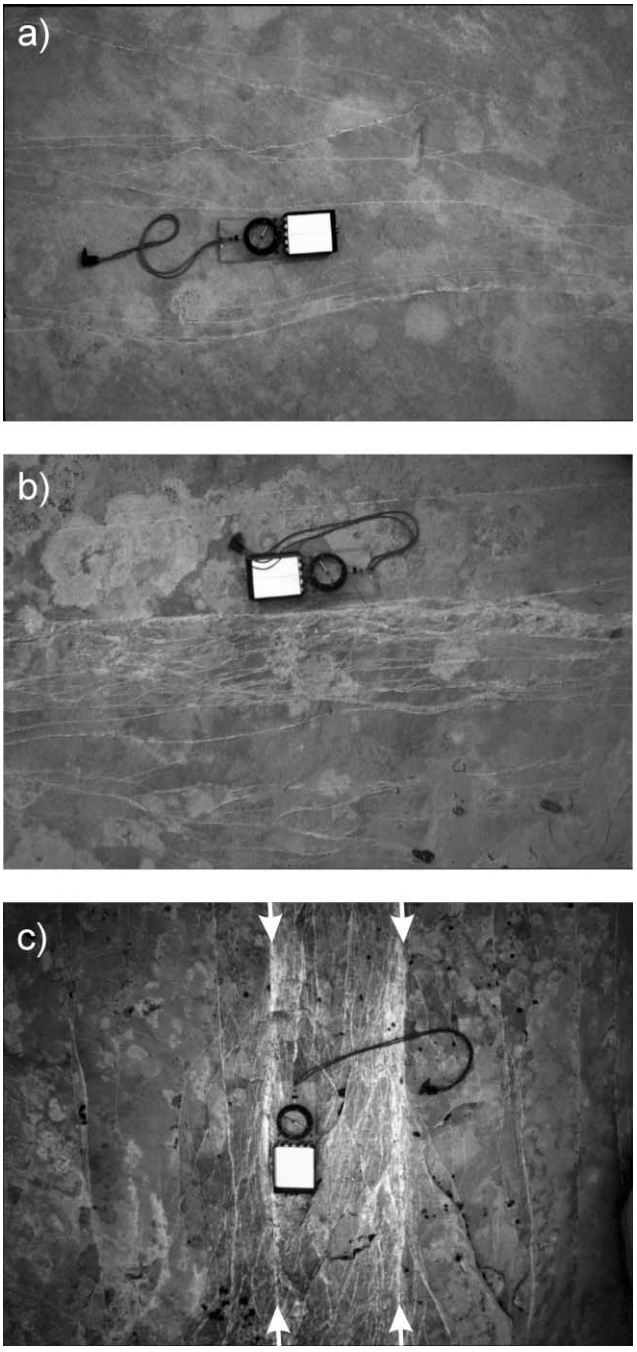

Fig. 3. Examples of the three cluster classes used in creating the damage zone maps. (a) Class 1 clusters: a few single and multi-strand bands but no slip-surfaces. (b) Class 2 clusters: several single and multi-strand bands with occasional, relatively discrete slip-surfaces. (c) Class 3 clusters: many single and multi-stand bands and complex anastomosing slip-surfaces. White arrows mark the position of slip-surfaces.

3. Methods and observations

3.1. Throw profiles

Throw profiles along both faults were constructed by mapping marker horizons in the Carmel Formation using a total station surveying instrument to build up geological maps of the fault zones. These acted as base maps for surveys of the damage zone structures and allowed the construction of stratigraphic separation diagrams by extrapolating strike lines into a vertical plane. To a first approximation, the throw is simply the height difference between the hangingwall and footwall cut-offs. Errors will be introduced due to the assumption that strata are planar on either side of the fault. The error due to uncertainty in bedding strike increases in proportion to the distance of the survey point away from the fault. Thus the error at the Big Hole Fault (±5–10 m) is greater than the error for the Blueberry Fault (±5 m) (Fig. 2). Furthermore because the measurement points are on bedding surfaces outside the damage zone, the throw profiles represent the sum of all the offsets in the damage zone in addition to that on the main fault surface. It is not possible to map out the vertical variation in throw from the field exposures. Thus the exposure of the fault trace represents a chord across the 3D fault plane that may be above or below the point of overall maximum throw. We have been unable to place constraints on this.

The throw profile for the Blueberry Fault tip [Fig. 2(a)] shows a linear decrease of throw with distance towards the tip (Cowie and Shipton, 1998). When the data for all four stratigraphic horizons are fitted with a straight line it has a slope of 0.015. This falls within the range of tip gradients in published literature, which range from 0.002 to 0.25 (Cartwright and Mansfield, 1998; Fossen and Hesthammer, 1997; Muraoka and Kamata, 1983; Peacock and Sanderson, 1996; Dawers et al., 1993; Walsh and Watterson, 1989; Schlische et al., 1996) and falls within the range of gradients for the Chimney Rock Fault array (0.005–0.05) calculated from the data of Krantz (1988b).

The throw profile for the Big Hole Fault [Fig. 2(b)] has a maximum at the centre of the fault and decreases linearly towards the eastern tip. The best-fit line for these data has a gradient of 0.014 [Fig. 2(b)]. Within error, this gradient is the same as that of the Blueberry Fault. To the east of the last point in our survey (1420 m from the centre of the fault), a step in the ground surface runs parallel to the projected position of the fault for 350 m. Three boreholes drilled by Shipton et al. (2001, in press) encountered the fault at 60 m depth at this site (1770 m from centre). Beyond this point the fault is buried beneath Quaternary sediment. No evidence of faulting is seen in an outcrop of the Entrada Sandstone 900 m to the east. The combination of the above observations indicates that the position of the tip can be constrained to 2046 ± 100 m from the point of maximum throw [Fig. 2(b)].

3.2. Macroscopic damage zone structures

The damage zone of the Big Hole and Blueberry Faults consists of clusters of deformation bands and slip-surfaces. The distribution of these clusters was mapped using the total-station surveying instrument. Clusters were classified into three size classes, depending on the number and size of

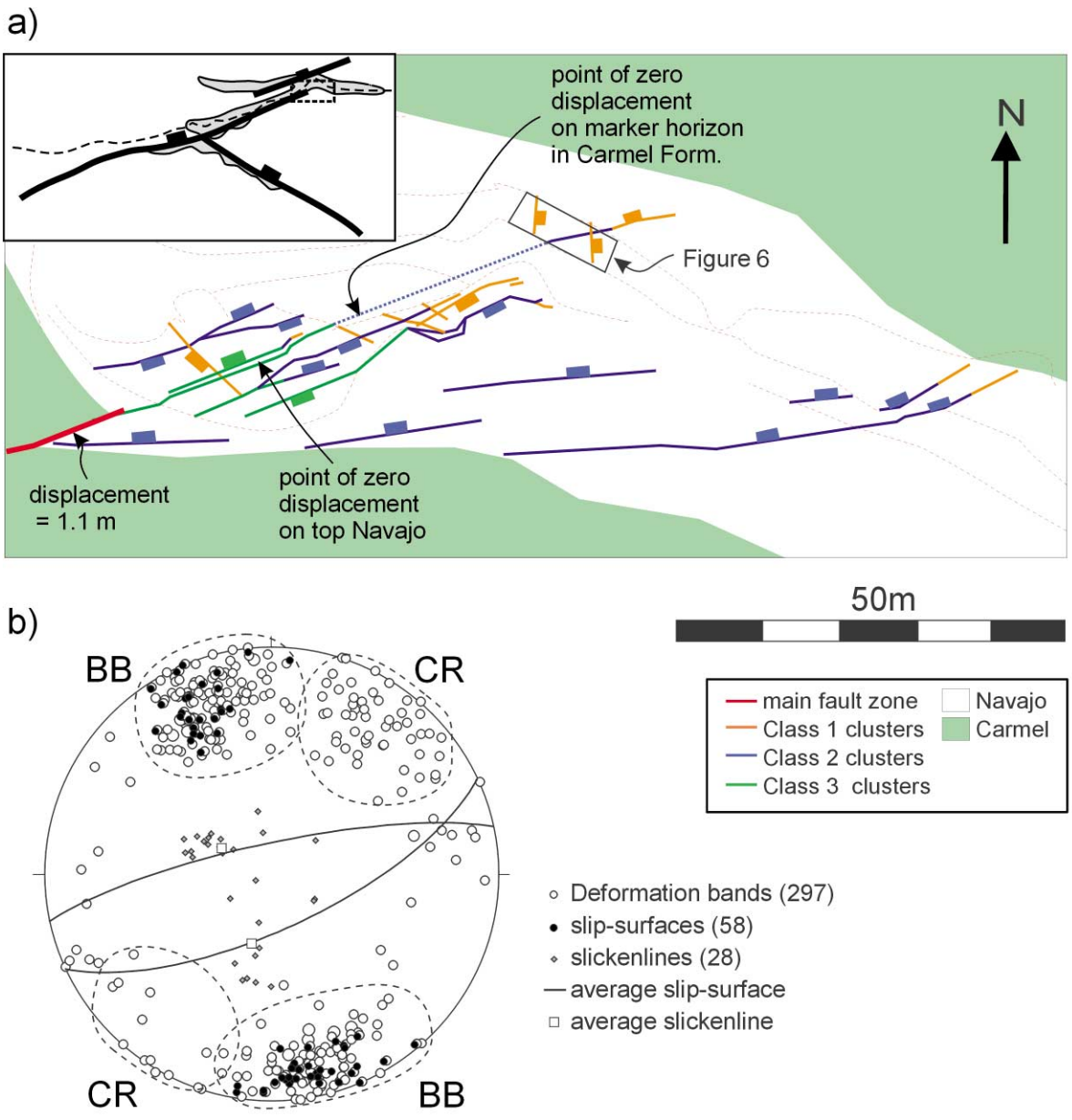

Fig. 4. (a) Map of deformation band clusters around the Blueberry Fault tip region. A tick marks the downthrown side of each cluster. Dotted lines represent breaks in slope or cover. The location of the outcrop-scale map (Fig. 6) is marked. The point of zero displacement as defined by two of the marker horizons is indicated. (b) Orientation of structures around the Blueberry Fault. Four clusters of deformation bands are seen, two parallel to the trend of the Blueberry Fault (BB) and two parallel to the second strike set of the Chimney Rock Fault array (CR). Slip-surfaces are only developed in clusters parallel to the Blueberry Fault. The great circles represent the average slip-surfaces synthetic and antithetic to the fault. The average slickenlines rake 20° to the west of pure dip-slip.

deformation bands in the cluster (Fig. 3). Each size class is defined by the average number and type of bands in a cluster. Within an individual cluster the majority of the deformation bands dip in the same direction. There is considerable lateral variability in the number and connectivity of the deformation band clusters so that transects taken a few metres apart along the same outcrop can have a significantly different form. Therefore, maps and sections that characterise the two-dimensional damage zone structure are much less ambiguous to interpret than linear transects through the damage zone.

The Blueberry Fault damage zone geometry was mapped from ahead of the tip to the point where the throw is 1.1 m (Fig. 4). At the point where the exposed fault trace intersects the top of the Navajo Sandstone (throw of 1.1 m) the fault consists of a well-developed slip-surface with dip-slip and minor oblique-slip striations. The point where the fault no longer has a well-defined slip-surface corresponds to the point where our measured throw approaches zero (the fault tip). Deformation band clusters to the east of this point contain only short, unlinked, slip-surfaces. One deformation band cluster is co-planar to the main Blueberry

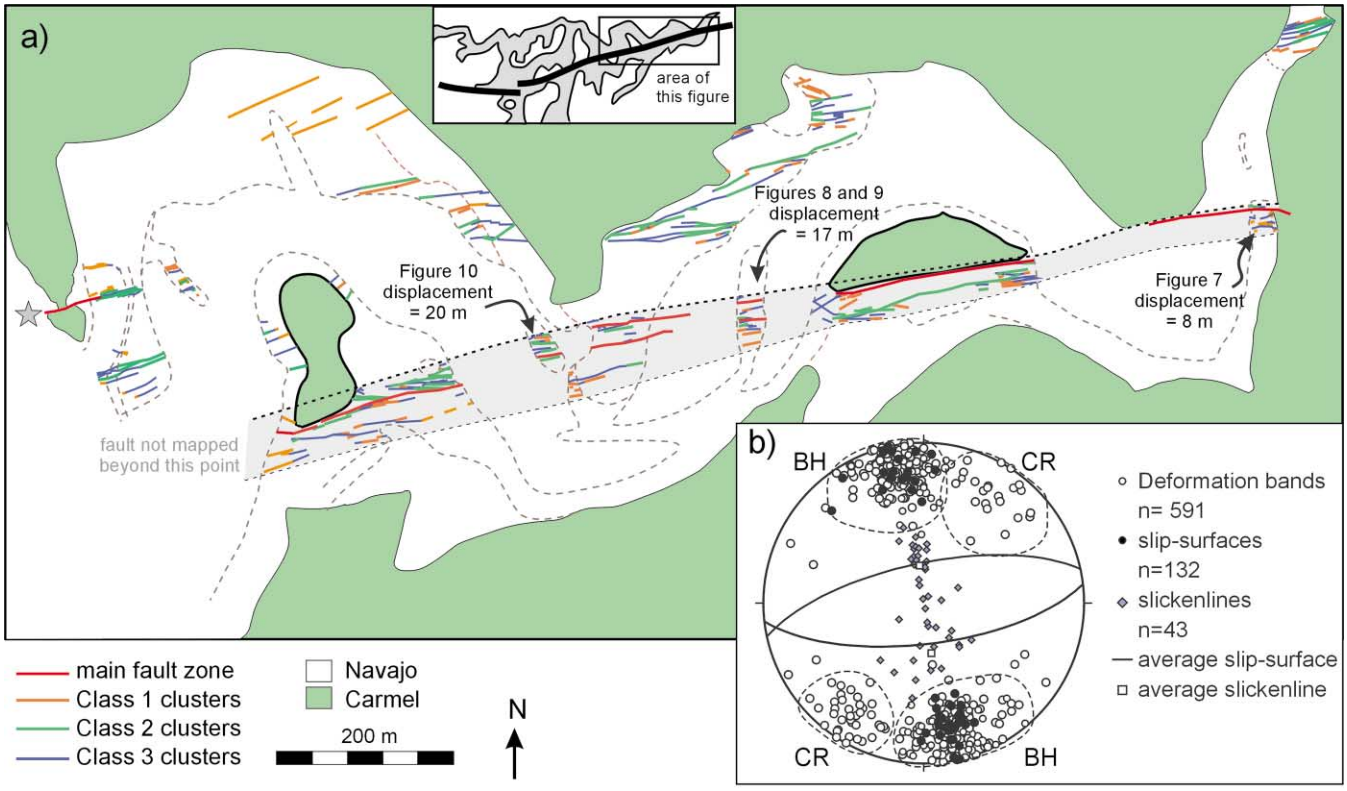

Fig. 5. (a) Map of deformation band clusters around the Big Hole Fault. Dotted lines represent breaks in slope or cover. The locations of Figs. 7–9 are marked. (b) Orientation of structures around the Big Hole Fault. Four clusters of deformation bands are seen, two parallel to the trend of the Big Hole Fault (BH) and two parallel to the second strike set of the Chimney Rock Fault array (CR). Slip-surfaces are only developed in the Big Hole Fault parallel clusters. The great circles represent the average slip-surfaces synthetic and antithetic to the fault. The average slickenlines are exactly dip-slip.

Fault, and two antithetic clusters dip to the south (Figs. 4 and 6). Beyond 45 m ENE of the point of zero throw no further structures are seen. The majority of deformation bands in the damage zone near the tip strike sub-parallel to the fault but some strike parallel to the second strike direction, described by Krantz (1988) for the overall Chimney Rock Fault array [Fig. 4(b)]. All of the slip-surfaces strike sub-parallel to the fault. Slip-surfaces near the fault tip have oblique striations pitching ~70° west [Fig. 4(b)].

The Big Hole Fault damage zone was mapped from its centre to the eastern limit of exposure [Fig. 5(a)]. The fault consists of a single fault strand for most of its length, although where the throw is between 12–20 m, slip is localised onto two left-stepping strands. The main fault surface is surrounded by a zone of deformation band clusters, but beyond a certain distance from the fault, only a few scattered deformation bands are seen. This enables us to define the width of the damage zone [Fig. 5(a)]. The majority of the deformation bands and all the slip-surfaces are strike-parallel to the fault [Fig. 5(b)] with approximately equal proportions of synthetic and antithetic structures. There is no difference in the orientation of structures between the footwall and hangingwall. A minority of deformation bands strike parallel to the second strike set of the main Chimney Rock Fault array [Fig. 5(b)]. These consistently cross-cut the fault-parallel structures, and we interpret them to be a later stage of deformation not associated with the growth of the Big Hole Fault. On average, slip-surfaces in the damage zone of the Big Hole Fault have pure dip-slip slickenlines.

3.3. Mesoscopic damage zone structures

Maps of individual outcrops were created by outlining a metre-square grid on the outcrop, and drawing the deformation bands directly onto graph paper. In this way the pattern of deformation bands can be recorded quickly and accurately. The deformation band maps were subsequently used to record the position of slip-surfaces. Although care was taken to include all the structures within complex clusters, the maps under-represent the true number of deformation bands in densely deformed regions. Areas of very high deformation band density, or where the deformation bands have effectively amalgamated together, are shaded in dark grey. Individual deformation bands often have small (1–5 cm long) sections where the band is locally thicker (>5 mm thick). Although care was taken to include these structures on the maps, some may have been omitted. No fractures smaller than a single deformation band are visible by eye so there is no lower resolution cut-off in size of feature on these maps. Maps were made at the tip of the

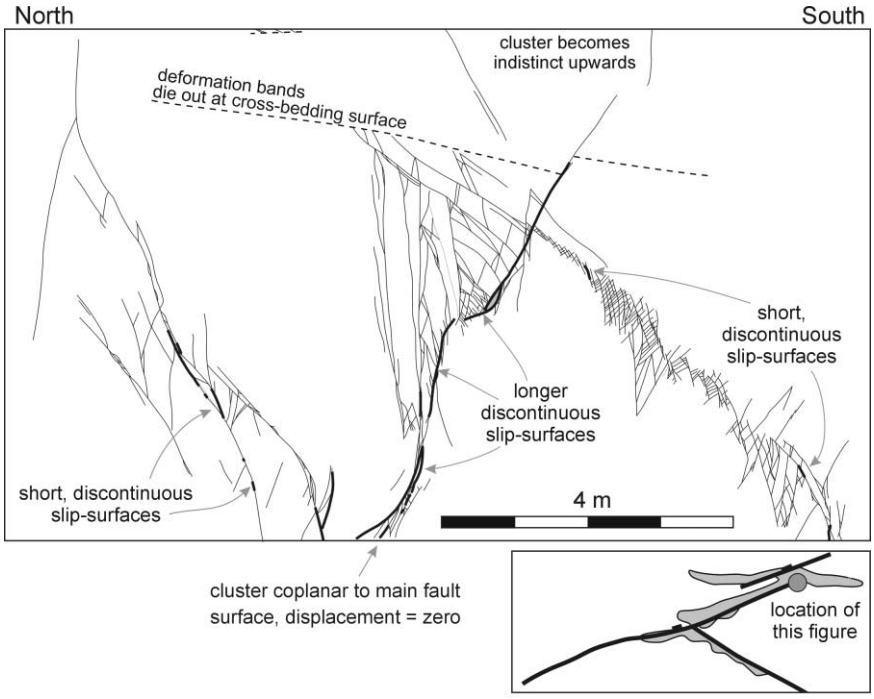

Fig. 6. Vertical outcrop map of the northern wall of the Blueberry Fault tip canyon (displacement = 0 m). Thin lines are deformation bands, thick lines are slip-surfaces, dotted lines are major bedding surfaces, the grey area in the centre is a slip surface.

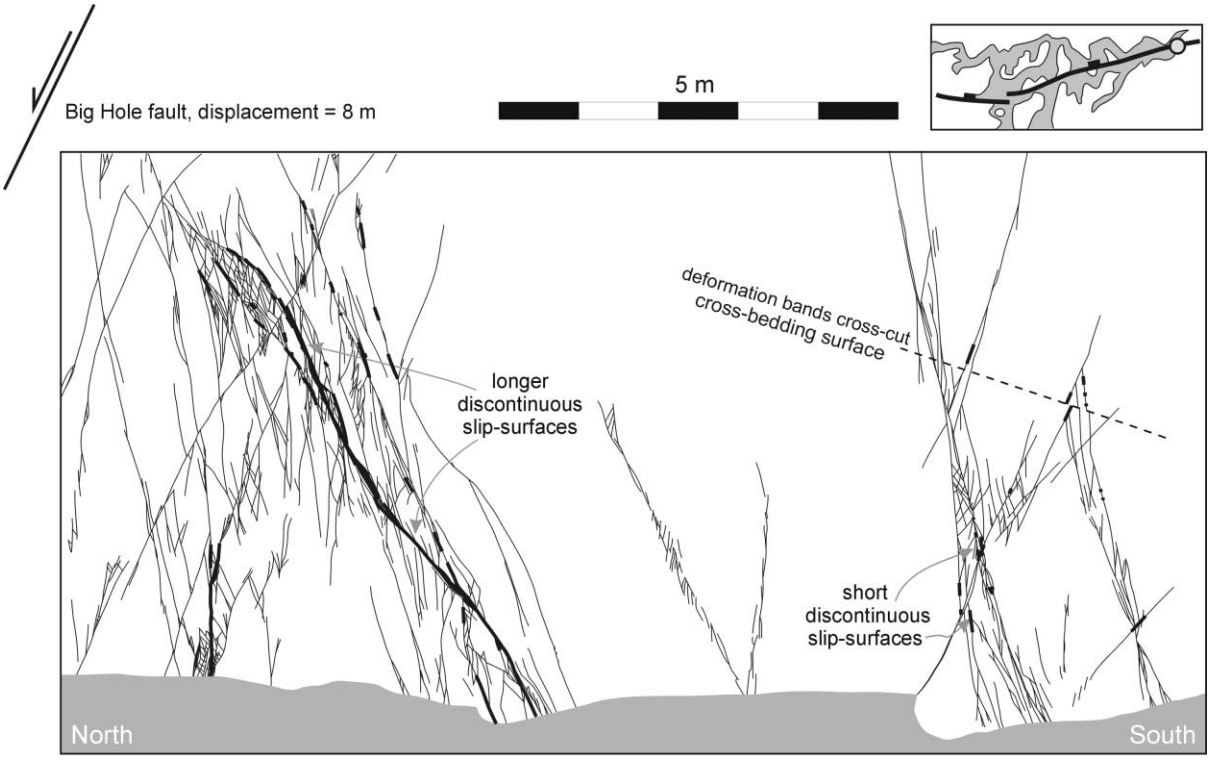

Fig. 7. Sub-vertical outcrop map of the footwall block at the easternmost outcrop of the Big Hole Fault (displacement = 8 m). Thin lines are deformation bands, and thick lines are slip-surfaces. Grey areas are sand at the base of the outcrop. The dotted line on the right-hand-side of the diagram is a bedding surface along which the deformation bands have been offset. The Big Hole Fault surface is off the left-hand-side of this map.

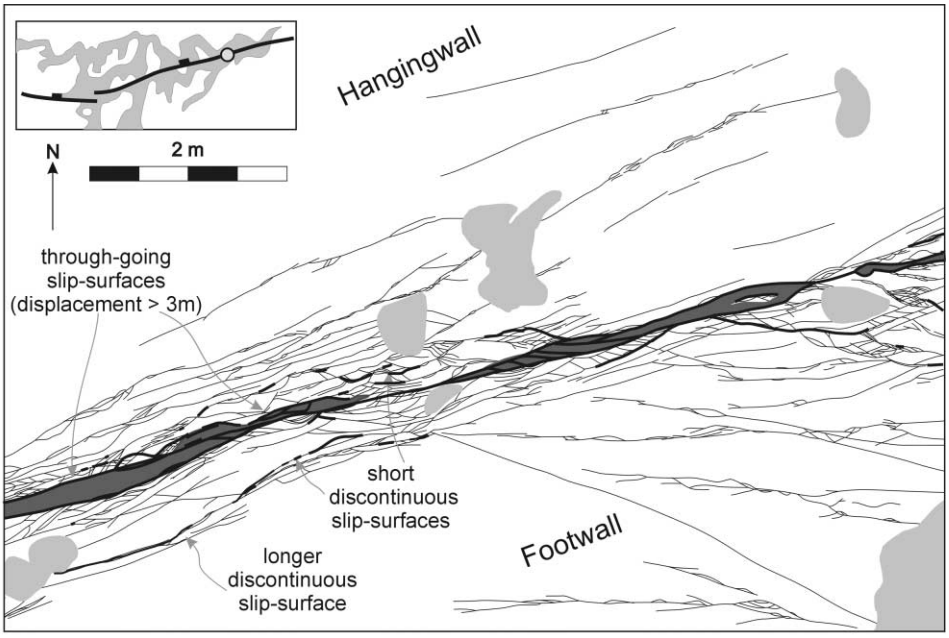

Fig. 8. Horizontal outcrop map of the northern strand of the Big Hole Fault at the location where the fault has two main strands (total displacement = 17 m). Thin lines are deformation bands; thick lines are slip-surfaces. Grey areas are complex zones of tightly packed deformation bands in which it is difficult to distinguish individual bands. Paler grey areas are covered with sand.

Blueberry Fault (throw <1 m) and at three locations along the Big Hole Fault, where the fault has 8, 19, and 24 m of throw.

At the Blueberry Fault tip structures were mapped in a sub-vertical canyon wall (Fig. 6). The cluster that is co-planar to the main Blueberry Fault consists of sub-parallel deformation bands and slip-surfaces merging upwards into a cross-hatched pattern of steeply dipping synthetic, and shallower dipping antithetic, deformation bands. A well-developed slip-surface runs up through the centre of this cluster but this and other structures die out at the top of the outcrop. The southern antithetic cluster (right-hand-side, Fig. 6) consists of a similar cross-hatched pattern of deformation bands. Only a few short (<10 cm) slip-surfaces occur within this cluster. The northern antithetic cluster (left-hand-side, Fig. 6) also has a cross-hatched pattern, but consists of longer, more widely-spaced deformation bands. Only one of these contains a well-developed, 1 m long slip-surface. In places the deformation bands terminate at bedding planes within the Navajo Sandstone. This is especially obvious in the hangingwall of the central cluster, where many bands terminate at a pronounced aeolian cross-set within the Navajo Sandstone. The main slip-surface, however, cuts through this bedding surface. None of the slip surfaces at this locality cut all the way through the outcrop, i.e. they are confined to within the Navajo Sandstone.

At the easternmost outcrop of the Big Hole Fault, where the throw is 8 m, the footwall is exposed in a cliff sloping 40–80° to the west (Fig. 7). The structures immediately adjacent to the fault and in the hangingwall are obscured by vegetation and so were not mapped. The main antithetic cluster in the footwall contains many discontinuous slip-surfaces (left-hand-side, Fig. 7). Two smaller antithetic clusters to the south contain short segments of slip-surfaces (right-hand-side, Fig. 7). These are often associated with local thickening of single deformation bands. This is a relationship that is seen throughout the field area. None of the slip surfaces in the footwall of the fault at this locality cut through the entire outcrop. Structures in the antithetic and synthetic clusters are mutually cross-cutting, indicating that they are coeval.

At the locality where the Big Hole Fault has a total throw of 17 m, offset is partitioned between two fault strands that are exposed in a horizontal outcrop in the base of the wash (Figs. 8 and 9). From the offset of the top Navajo Sandstone to the east the throw can be constrained to a minimum of 3 m on the northern strand (Fig. 8) and a maximum of 14 m on the southern strand (Fig. 9). In contrast to the tip outcrop (Fig. 6), single slip-surfaces can be traced through the northern fault strand (Fig. 8). Other slip-surfaces anastomose around this main one, defining the edges of a zone of concentrated deformation (shaded area in Fig. 8). The width of this zone is highly variable from a single slip-surface in the centre of Fig. 8, to up to 30 cm wide on the left and right-hand-sides of Fig. 8. In the western half of the map (left-hand-side, Fig. 8) deformation bands extend about 1–1.5 m symmetrically to either side of the fault strand. In the eastern half of the map (right-hand-side, Fig. 8) the deformation is mostly within the footwall. The southern strand (Fig. 9) consists of many anastomosing slip-surfaces. Dense clusters of deformation bands occur close to the fault

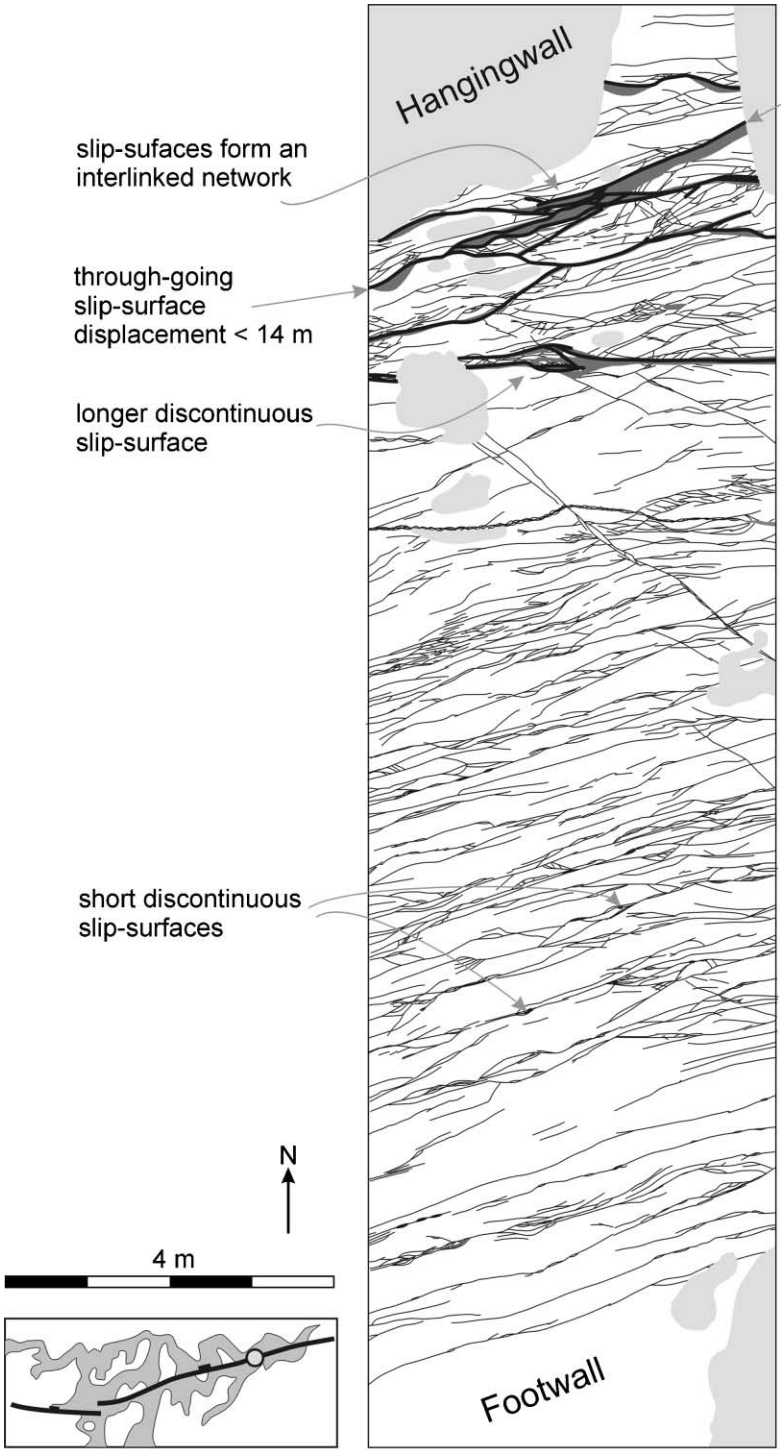

Fig. 9. Horizontal outcrop map of the southern strand of the Big Hole Fault at the location where the fault has two main strands (total displacement = 17 m). Key as in Fig. 8. Arrows mark the main fault surface.

in the hangingwall and footwall. Complex clusters of single and multi-strand deformation bands occur up to 14 m into the footwall.

Where the Big Hole Fault has 20 m of throw a single main fault surface is exposed in a sub-horizontal outcrop at the base of the wash (Fig. 10). Discontinuous slip-surfaces anastomose alongside the main surface, which cuts through the entire outcrop. This defines a zone of concentrated deformation about the main fault (dark grey in Fig. 10) that varies from 10 to 30 cm wide along strike. In the footwall of the fault there is one large antithetic cluster, in the hangingwall several large clusters are seen up to 26 m from

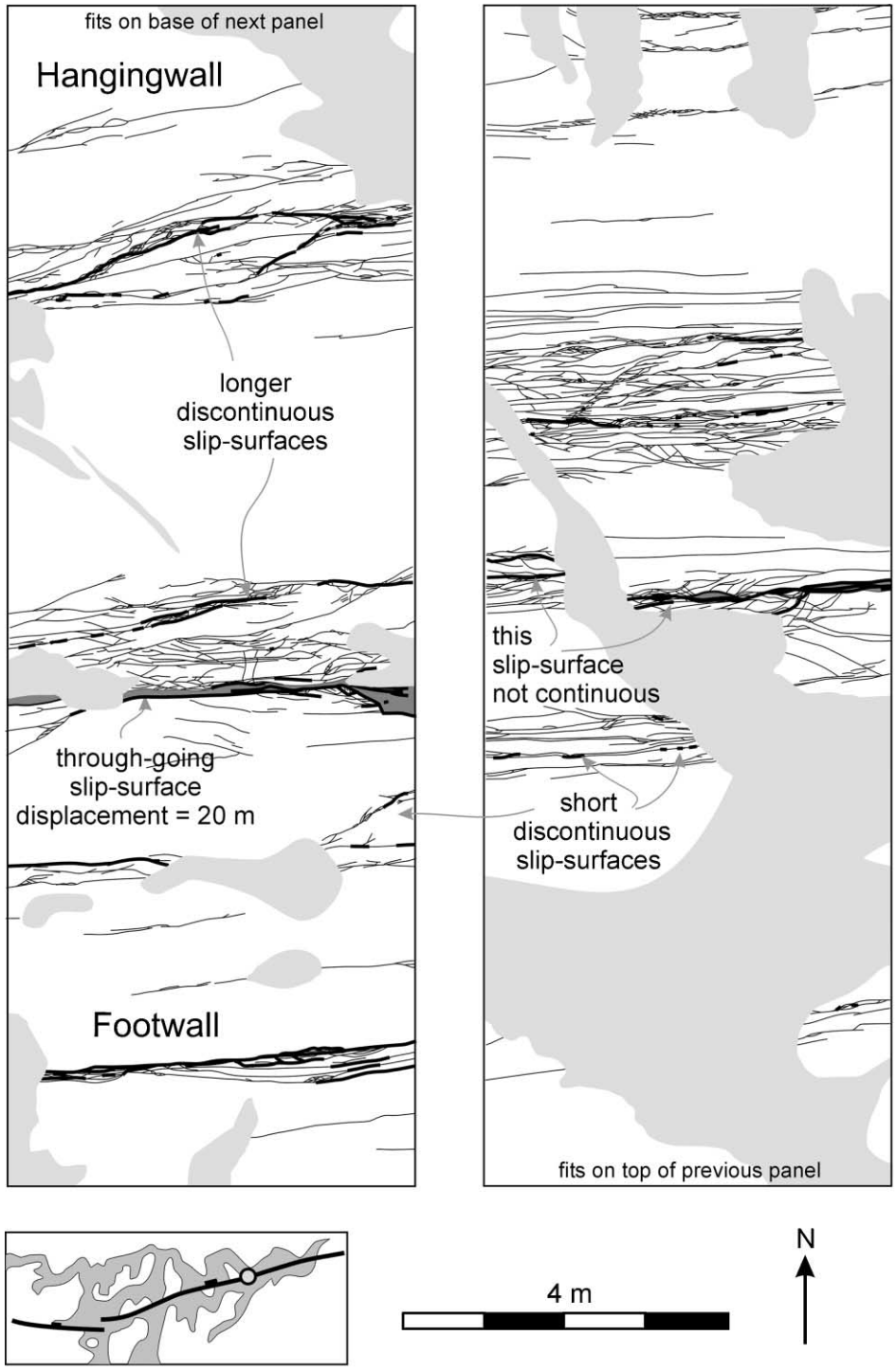

Fig. 10. Horizontal outcrop map of the Big Hole Fault where it has a single main fault strand (displacement = 20 m). Key as in Fig. 8. Arrows mark the position of the main fault surface. The right-hand map fits onto the bottom of the lift-hand map.

the fault. Only two of these clusters contain a significant number of slip-surfaces but these are not laterally continuous.

3.4. Microscopic damage zone structures

Thin sections of deformation bands and host rock were examined under an optical microscope, and with cathodoluminescence (CL) and backscatter (BSEM) modes on an electron microscope. As seen in previous studies (Aydin, 1978; Aydin and Johnson, 1978; Mair et al., 2000), single deformation bands consist of broken, angular, grain fragments supporting relatively unbroken host-sized grains, in a narrow band approximately 1 mm wide and have reduced

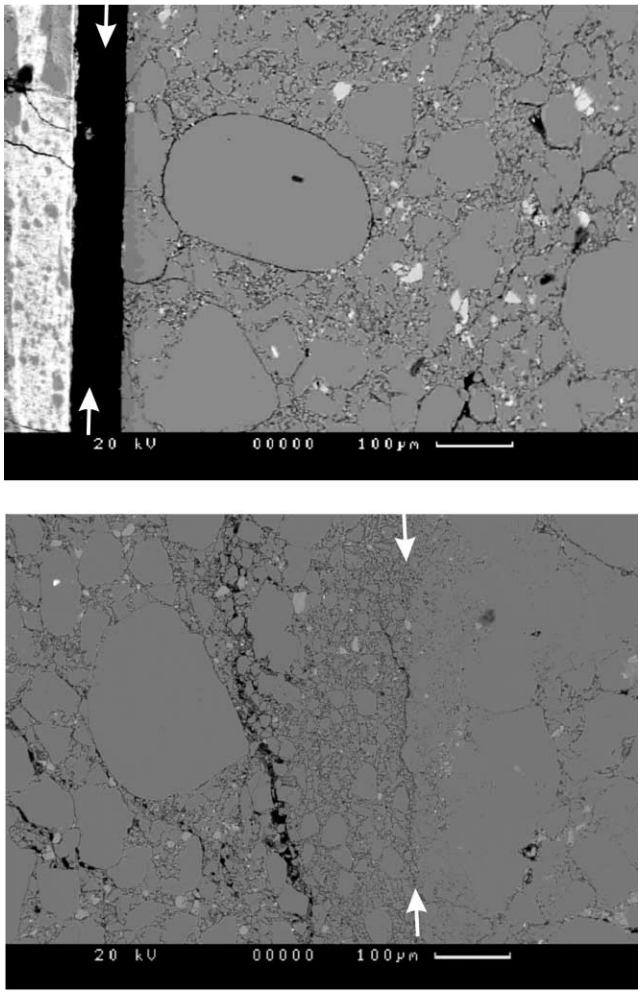

Fig. 11. (a) BSEM image of the through-going slip-surface that is considered to have accommodated the majority of the displacement at the 24 m location. The slip-surface sits within a zone of intense grain crushing. There is some cement at this locality (pale grey). (b) BSEM image of a slip-surface near the Blueberry Fault tip (zero displacement) within a zone of intense grain crushing. Note that although the degree of grain crushing is similar, the slip-surface is not as well developed as the 24 m one.

grain size and sorting with respect to the host rock. Zones of deformation bands consist of several anastomosing bands with essentially identical microstructures. Pods of relatively undeformed host rock with little or no grain crushing are preserved between the bands.

Slip-surfaces are always located within intensely crushed zones between 1 and 2 mm wide. Fig. 11(a) shows the slip surface that has accommodated the majority of the 20 m throw at the location in Fig. 10. Despite the proximity to a major slip surface, relatively intact grains are still seen, but individual grains have been planed off as offset was accommodated along this surface. These grains sit within a tightly packed matrix of crushed grains. Fig. 11(b) shows part of a short, discontinuous slip surface from near the tip of the Blueberry Fault (Fig. 6). This is not a through-going slip-surface, and although it does sit within a zone of highly crushed rock, it does not have the very straight edges characterising longer, higher offset surfaces. The small grain size around slip-surfaces that are just nucleating implies that grain crushing is an early stage in the formation of slip-surfaces.

Microfracture density was determined using a method similar to that of Anders and Wiltschko (1994) and Vermilye and Scholz (1998). The number of fractures crossing a 0.15 mm transect line is recorded. Grains smaller than half a cross hair are not counted. The numbers of microfractures in 40 grains were counted across each sample and the number of microfractures per millimetre is then averaged for each transect. A U-stage (used to detect microfractures at lower angles to the thin section plane) was not used in this study so the true number of microfractures will be underestimated. However the underestimate will be consistent for all samples and we are more concerned with variations of microfracture density across the damage zone. The microfracture densities in this study are similar to data from the same rock type determined by Anders and Wiltschko (1994) using a U-stage.

No decay of microfracture density is seen with distance from the fault (Fig. 12). The average microfracture density away from deformation bands is 9.65 mm^{-1}. The average microfracture density for samples within 0.5–1 cm of a deformation band is 12.47 mm^{-1}. However, the two datasets are statistically indistinguishable, showing that there is no increase of microfracture density above host rock values adjacent to deformation bands (Fig. 12). The majority of microfractures occur within the grains and do not cross between grains. Most are straight, and do not appear to be controlled by the position of grain boundaries. Mair et al. (2000) found microfractures up to a few grain widths either side of experimentally generated deformation bands. They suggested that the absence of visible microfractures in real deformation bands is due to healing. However the use of CL in our study has shown that in grains that have quartz overgrowths the microfractures stop at the original grain boundaries and do not extend into the overgrowths implying that this diagenesis occurred later than the formation of these microfractures. The absence of any correlation between microfracture density and distance from the fault suggests that these microfractures are not related to movement along the fault surface.

4. Damage zone width and geometry

It is relatively straightforward to define a damage zone width for the Big Hole and Blueberry Faults; deformation bands are clustered around the fault, and beyond a certain distance there are essentially no deformation bands. A subsidiary zone of deformation bands clusters is observed between 150 and 200 m into the hangingwall of the Big Hole Fault (Fig. 5). It is conceivable that these structures could be linked along strike to form a continuous cluster. However, except at one location (marked with a star on Fig. 5), no offset of the top Navajo Sandstone is associated with this cluster. It is interesting to note that where the Big

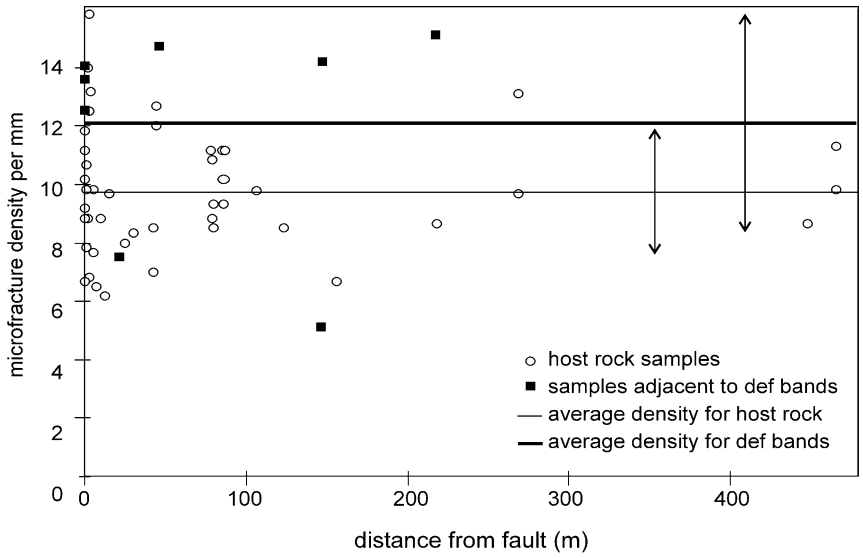

Fig. 12. Comparison of microfracture densities in the host rock (open circles) and for samples within 0.5–1 cm of a deformation band (filled squares). The mean microfracture densities for the host rock and adjacent to deformation bands are shown as solid lines. The arrows indicate one standard deviation either side of the mean.

Hole Fault has two strands, the southern strand is surrounded by more deformation band clusters than the northern strand. The southern strand is likely to have a higher throw. This implies that the width of the damage zone and/or the density of structures in the damage zone away from the fault correlates with fault throw. This apparent correlation between damage zone width and throw is investigated in the discussion.

The number of slip-surfaces at each location was counted from the outcrop sketches. Four slip-surfaces cut the base of the Blueberry Fault tip outcrop (Fig. 6), three cut the 8 m throw outcrop (Fig. 7), ten cut the 17 m throw outcrop (Figs. 8 and 9) and eleven cut the 20 m throw outcrop (Fig. 10). These results point towards a positive correlation of the number of slip-surfaces with the throw on the main fault surface, but we need to collect more data to confirm this. At the higher throw outcrops slip-surfaces seem to be concentrated within the clusters closest to the fault and the number and continuity of slip-surfaces decreases away from the fault (for example, see Fig. 10).

Oblique-slip slickenlines occur throughout the Blueberry Fault tip outcrop (from 0–23 m from tip, 0–1.1 m of throw). However, dip-slip slickenlines are dominant at the Big Hole Fault outcrop that has 8 m of throw (500 m from tip). If the fault has propagated by radial propagation (e.g. Cowie and Scholz, 1992), the almost total lack of oblique-slip slickenlines on the Big Hole Fault surface suggests that repeated

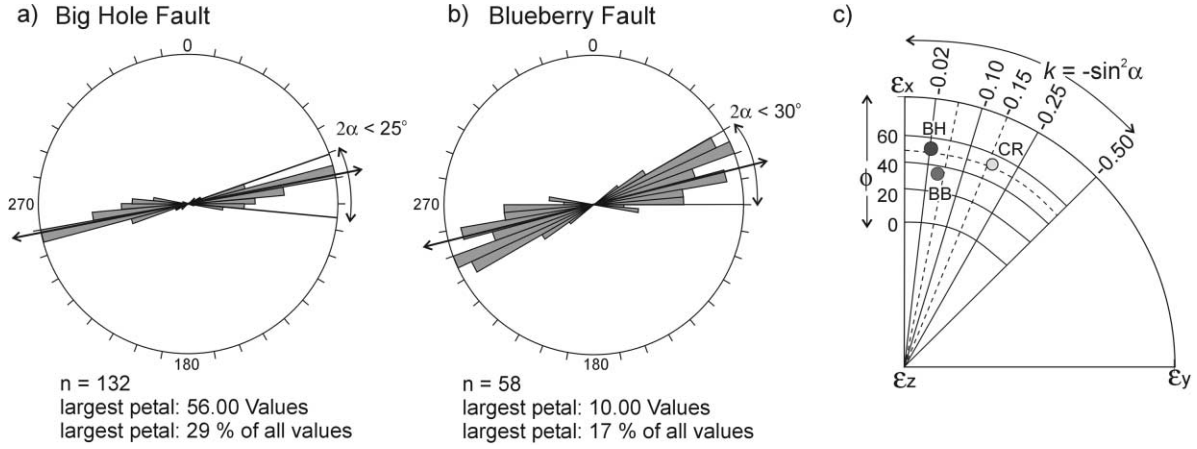

Fig. 13. Rose diagrams of the strike of slip-surfaces in the off-fault deformation around (a) the Big Hole Fault and (b) the Blueberry Fault showoing that the scatter in strike is approximately symmetrical around the main fault surface (arrows show the strike of the main fault) and that the scatter is greater around the Blueberry Fault than around the Big Hole Fault. (c) Slip model net showing data points for the Big Hole Fault (BH), the Blueberry Fault (BB) and the Chimney Rock Fault array (CR).

slip on the fault obliterates evidence of oblique slip at the fault tip. The oblique-slip slickenlines must be obliterated at some point between 1 and 8 m of throw. Roberts (1996), Morewood and Roberts (1997, 2000) and Wu and Bruhn (1994) documented similar along-strike changes in slip vector at fault segment boundaries and suggested that this reflected local strain patterns at fault segment tips. In cases of limited exposure, the presence of oblique-slip slickenlines on an otherwise dip-slip fault could be a useful indicator of the proximity to the fault tip.

5. Orthorhombic geometry of the damage zone

The scatter in deformation band strike is approximately symmetrical around the main fault surface [Fig. 13(a) and (b)]. In plan view, deformation bands are not strictly parallel to one another, defining thin lozenge-shaped blocks of relatively undeformed sediment between deformation bands (Figs. 8–10). In cross-section, structures within the damage zone form a conjugate geometry (Figs. 6 and 7). Thus, it appears that the structures within the damage zone exhibits an orthorhombic geometry, comparable to the overall orthorhombic pattern shown by Krantz (1988a) for the entire Chimney Rock array, but with a lower angle between strike sets. We have used the method of Krantz (1988a) to identify and quantify the three-dimensional strain field represented by the structures within the damage zone.

The slip model developed by Reches (1978, 1983) and elaborated by Krantz (1988a), assumes that all the strain in a deforming region is accommodated along faults, following Coulomb frictional behaviour. For conjugate faults, the angle between fault sets is 2θ, where $2\theta = (90 - \phi)$ and ϕ is the angle of internal friction. Within each strike set of a orthorhombic normal fault array the dip of the faults is the same as that for a conjugate pair. However the acute angle between the strikes of each set, α, is a function of the ratio of the intermediate to minimum strains, k. The value of k can range from -0.5 (oblate strain) to 1 (prolate strain), with plane strain occurring when $k = 0$. For normal faults, α is given by

$$k = -\sin 2\alpha \quad (1)$$

This simplified relationship is demonstrated byKrantz (1988a,b) to be true for fault sets where the ratio of fault throw to fault spacing is small.

For our data an upper limit on the value of α is the acute angle between the extremes of the scatter in strike directions [Fig. 13(a) and (b)]. For the Big Hole Fault data, the scatter in strike direction defines a maximum value for 2α of 25° ($k < -0.05$). The scatter in the strike directions for the Blueberry Fault tip places an upper limit on 2α of 30° ($k < -0.07$). When the data are plotted on a slip model net for normal faults [Fig. 13(b) and Reches, 1983] the value of k and ϕ can be read directly (for a detailed discussion of this method see Krantz, 1988a, 1989). For the entire regional Chimney Rock Fault array $k = -0.16$ ($\alpha = 24°$) and $\phi = 54°$ (Krantz, 1988a). For the Big Hole Fault damage zone deformation $k = -0.02$ ($\alpha = 8°$) and $\phi = 53°$. For the Blueberry Fault the slip model net defines a k value of -0.04 ($\alpha = 11.5°$) and a ϕ of less then 40°. The value of ϕ for the Big Hole Fault is consistent with the data for the Chimney Rock Fault array as a whole, which would be expected given that it formed in the same rock type. The value of ϕ at the Blueberry Fault tip is lower, which is not realistic since it is within the same lithology. However the value of phi is less well constrained for the Blueberry Fault due to the scatter in slip-surface orientations (Fig. 4). The difference in k, however, is resolvable and clearly shows that k is significantly lower in the damage zones of these faults compared to the entire Chimney Rock Fault array. The larger value of k (closer to zero) for the Big Hole Fault damage zone structures is still consistent with three-dimensional rather than plane strain, but indicates that the strain is less oblate than that at the Blueberry Fault tip.

It has been suggested that along-strike extension due to flexure of the hangingwall and footwall occurs to accommodate increasing offset on the fault (Wu and Bruhn, 1994; Roberts, 1996). This strain can be estimated for the Big Hole Fault by assuming (1) bedding was originally horizontal, (2) a triangular throw profile and (3) symmetrical footwall uplift and hangingwall subsidence. For these assumptions, the fault parallel strain is in the order of 3×10^{-5}. The value of k resulting from the odd axis and slip models for both the Big Hole Fault and the Blueberry Fault would indicate that the fault perpendicular strain is between 30 and 50 times the fault parallel strain, i.e. in the order of 0.9×10^{-3} to 1.5×10^{-3}. One-dimensional transects through the damage zone (at the same locations as the outcrop maps) allow us to calculate the fault perpendicular strain (Shipton, 1999). These values are obtained by summing the measured and estimated throw on all structures encountered on each transect. The value of strain from these calculations is 8.7×10^{-3} (Shipton, 1999), which is of the same order of magnitude as that calculated from the orthorhombic geometry. Therefore, it is likely that the three-dimensional strain giving rise to the orthorhombic damage zone geometry is due to a component of along-strike strain, resulting from along-strike flexure of the hangingwall and footwall in addition to fault perpendicular extension.

The damage zone structures are therefore not growing in the regional strain field that produced the orthorhombic symmetry of the overall fault array (compare the damage zone geometries to the Chimney Rock Fault array on Fig. 1). Instead, the damage zone geometry is consistent with the local three-dimensional strain field around the Big Hole and Blueberry Faults, i.e. the strain field that is induced by accumulation of offset on a pre-existing fault plane. Therefore, in applying Krantz's approach, care must be taken to separate out those structures that formed due to local strain variations within the larger scale fault array, from the structures that formed in response to the regional strain field.

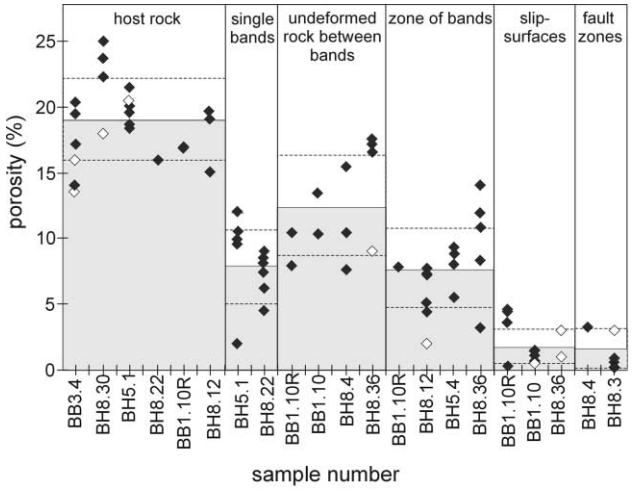

Fig. 14. Porosity as a function of deformation band evolution. The samples have been arranged according to deformation type. The shaded bars represent the mean porosity value for each deformation type and the dashed line presents one standard deviation. Filled symbols are measurements made with Erdas Imagine, unfilled symbols are measurements made with Optimas.

Moreover, this example clearly demonstrates the potential pitfall of extrapolating small-scale structural geometries to a regional scale.

The along-strike variation of slip vectors described above suggests that the geometry of deformation at the fault tip is different than that forming alongside a fault surface with larger throw. Although the values of k from the slip model nets are similar, the value of k indicated by the range in deformation band strike is larger for the Blueberry Fault tip than for the Big Hole Fault. This would indicate that the strain field is more oblate at the tip, and that subsequent slip on the fault promotes the growth of deformation bands in an orthorhombic pattern with a lower angle between strike sets. Morewood and Roberts (1997) found that strain was more oblate (lower values of k) at the tips of individual fault segments and closer to plane strain in the centre of faults. This suggests another way that the deformation at the fault tip could be distinguished from deformation alongside well-developed fault surfaces.

6. The fault core

The main Big Hole Fault zone, where throw is greater than 8 m, consists of a concentrated zone of deformation up to 30 cm wide with low grain size and porosity, bounded on one or both sides by slip-surfaces (shaded areas in Figs. 8–10). This zone, where slip is localised, is the fault core as defined by Chester and Logan (1986) and Caine et al. (1996). It has been argued that a scaling between the fault core width and throw exists (Hull, 1988; Evans, 1990). However, in this study the width of these zones appears to be independent of the throw on the fault, and significant variation is seen locally (on a sub-metre scale) along strike (Fig. 8 compare left- and right-hand-sides of this diagram).

Within the fault core, slip-surfaces can be identified that run through the entire length of individual Big Hole Fault outcrop maps (Figs. 7–10). These must be the surfaces upon which most of the offset has been localised, and therefore represent the main slip-plane of the fault itself. If no continuous slip-surface can be traced through a cluster, then no significant localisation of offset can have taken place. This provides a criterion for defining fault core clusters from clusters within the damage zone. Additionally, the discontinuous nature of slip-surfaces in the clusters around the Blueberry Fault is consistent with the observation that these structures represent deformation ahead of the fault tip, rather than on the well-developed fault surface.

7. Porosity and grain size reduction

The porosity of small regions within the samples was

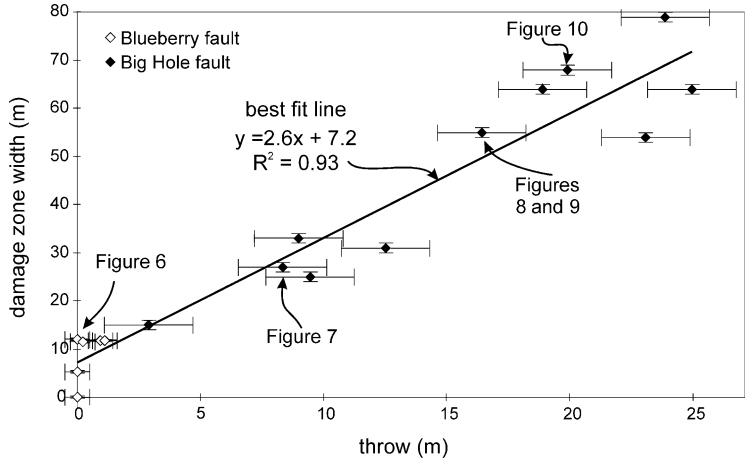

Fig. 15. Scaling of damage zone width (hangingwall and footwall summed) with displacement. The best-fit line is for both faults. The error in displacement is in the order of ±1 m for the Blueberry Fault and ±1.5 m for the Big Hole Fault. Errors in off-fault damage zone width are ±0.25 m for the Blueberry Fault and ±1 m for the Big Hold Fault. The location of the damage zone maps (Figs. 6–10) are indicated.

calculated by image analysis of BSEM images using two software packages: Erdas Imagine and Optimas. BSEM images have a strong contrast between the grains and the epoxy used for mounting the samples, and each mineral has the same grey level across the image, so no problem occurs with identifying minerals or distinguishing them from the epoxy. A correlation between the porosity and the amount of grain crushing has been observed in many studies of deformation band microstructure (Fowles and Burley, 1994; Mair et al., 2000). So a reduction of porosity in deformation bands with respect to the host rock can be correlated with the visible grain size reduction and reduced sorting due to cataclasis. There is no measurement error as such associated with individual image analysis porosity measurements; the porosity is the number of pixels below a certain grey scale divided by the total number of pixels in the image. Instead we show the standard deviation for each deformation style dataset in Fig. 14.

The average host rock porosity of 19.2% is typical of the Navajo Sandstone (Dunn et al., 1973). The mean porosity for single deformation bands (7.9%) and zones of deformation bands (7.4%) is not statistically distinguishable (Fig. 14). The grain size data of Mair et al. (2000) also show that the grain size distribution within the deformation bands did not change with the addition of successive deformation bands. These observations confirm the model of Aydin and Johnson (1978) that each deformation band in a zone is added as a discrete element, and imply that the mechanism forming each deformation band is essentially the same. Rock from between two bands in a zone of deformation bands, which appears undeformed in hand specimen, has a mean porosity of 11.9%, significantly lower than for the host rock. Mair (1997) also observed qualitatively that the porosity was lower in pods of host rock between bands, than for the host rock away from deformation bands. Pore collapse has probably occurred by compaction and re-organisation along grain boundaries, possibly enhanced by the presence of clay and haematite coatings on the grains.

Rock in the wall of slip-surfaces had the lowest average porosity (1.3%). Even more importantly, the porosity value does not show a systematic change or decrease with the amount of throw accommodated by the slip surface. For example, the lowest porosity (0.5%) was seen on the slip-surface at the Blueberry Fault tip, which has negligible throw. This value remains essentially the same for fault plane slip-surfaces with higher throw (an average of 1.5%). The rock adjacent to the slip surface where ~20 m of throw has been accommodated has 2.6% porosity (Fig. 14). It seems that porosity lies within a narrow range regardless of throw on the adjacent slip-surface. The observation that the porosity is substantially lower than that measured for deformation bands, suggests that the processes forming these two types of structures are different. In other words there is not a continuum of evolutionary states from a deformation band to a slip surface, but instead a distinct change in mechanism.

8. Discussion

8.1. Correlation between damage zone width and throw

Deformation bands are clustered around the Big Hole and Blueberry Faults, and beyond a certain distance only occasional isolated deformation bands are seen. This distance defines the edge of the damage zone (Figs. 4 and 5). The damage zone width around the Big Hole and Blueberry Faults is larger where the throw is greater. When we plot the damage zone width (hangingwall and footwall summed) against throw (Fig. 15), the data are reasonably fit by a straight line. According to this correlation, the damage zone width is approximately 2.5 times the throw. However, the error bars on Fig. 15 show that the predicted damage zone width could vary by about as much as 10–20% for any given value of throw. This correlation implies that deformation is still being accommodated within the damage zone after a through-going fault surface has developed. This conclusion is backed up by the orthorhombic analysis, which shows that the damage zone deformation is consistent with strain around a growing fault rather than with the regional strain field (Fig. 13).

A positive correlation of damage zone width and throw has also been found by Fossen and Hesthammer (2000), Beach et al. (1999) and Beach et al. (1997) (in Jurassic sandstones of the North Sea, the Nubian Sandstone in the Suez rift and Permo-Triassic sandstones in NW England respectively). Knott et al. (1996) found that damage zone half-width (in mixed lithologies) scaled with offset, but they found that the hangingwall and footwall had different distributions, which is not the case in our area. Roberts (1994), however, found that no strain accumulated within the damage zone of a shallow thrust as offset was accumulated. He interpreted this to mean that the fault had slipped aseismically due to its low burial depth (2–3 km). However, our faults and those in the Fossen and Hesthammer (2000) and Beach et al. (1999) studies developed at low burial depths and have accumulated deformation in the damage zone. The fault studied by Roberts (1994) developed in carbonates, which are presumably low-porosity. Increasing experimental evidence is showing that an important difference exists between deformation in high and low-porosity rocks (see Wong et al., 1997; Wong and Zhu, 1999 and references therein). Therefore, it is most likely that damage zone development is lithology dependent, and this should be taken into consideration when damage zone widths are analysed.

8.2. The process zone

Most discussions of deformation ahead of propagating fault tips have concentrated on microscopic deformation in the process zone (Scholz et al., 1993; Anders and Wiltschko, 1994; Vermilye and Scholz, 1998). The low microfracture densities seen in this study contrast with the

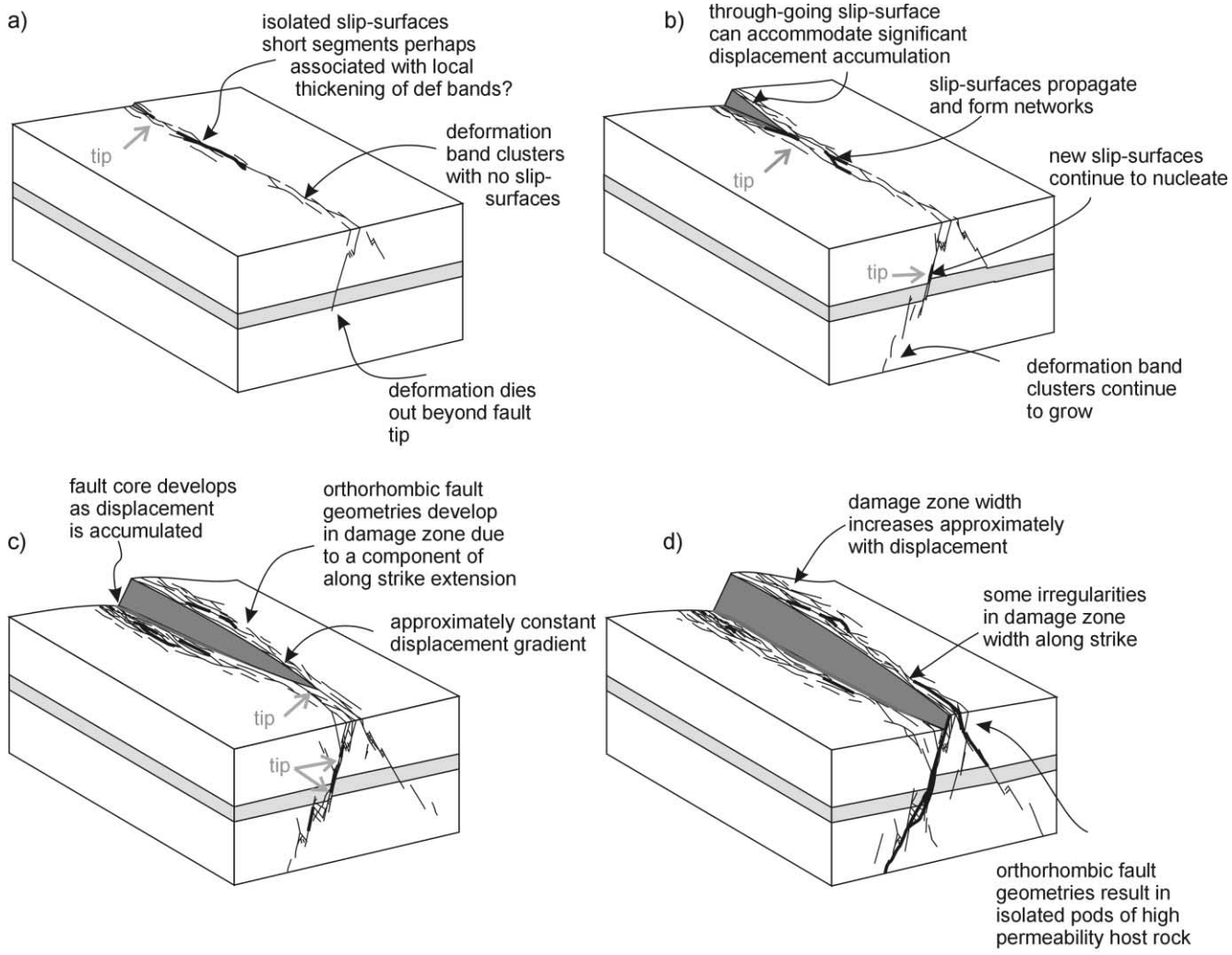

Fig. 16. Schematic illustration of a model for the growth of faults in porous sandstones. The cartoon illustrates the evolution of a fault in the same block of rock through time. Alternatively, it could represent successive along-strike sections of an inactive fault zone, as in this study. Grey arrows mark the position of the fault tip. (a) Deformation is taking place ahead of the tip in the form of deformation band clusters. Small patches of slip surfaces have nucleated within the deformation band clusters. (b) Principal slip surfaces have coalesced to form a through-going surface at the fault tip. The density of deformation band clusters increases, and new slip surfaces continue to form within deformation band clusters. (c) Further displacement accumulation is mostly along this through-going slip-surface. Some slip-surfaces continue to nucleate within the damage zone. (d) Deformation in the footwall or hangingwall of the fault (the damage zone) increases in width.

large numbers of fault-related microfractures described by Vermilye and Scholz (1998) in a highly indurated quartz sandstone and by Anders and Wiltschko (1994) in calcite and silica cemented sandstones. These data, for low-porosity rocks (porosity $<10\%$), describe a logarithmic decrease in microfracture density with distance from the fault. However, Anders and Wiltschko's (1994) data for the Navajo Sandstone and Entrada sandstones show a poor correlation with distance from the fault with no data above 9 microfractures per millimetre, comparable with our results (Fig. 12).

In low-porosity sandstones and quartzites the interlocking of grains promotes fracture of the grains rather than grain boundary fracture and rolling. Experimental studies report large numbers of acoustic emissions occurring throughout high-porosity sandstones before failure (Lockner et al., 1992). Thin section analysis of these experimentally deformed sandstones has shown that grain crushing caused by enhanced stress at grain contacts causes this lithology to fail and form deformation bands without the production of the dense population of intra-grain microfractures that was seen in granites (Lockner et al., 1992). The acoustic emissions have therefore been interpreted as the rupture of grain boundary microfractures. In the absence of any pre-faulting cement that could act as a marker for failure, the identification, and hence quantification, of grain boundary microfractures is extremely difficult, if not impossible, in mature sandstones such as the Navajo Sandstone. The presence of deformation bands ahead of the fault tip at the Blueberry Fault along with the low numbers of

microfractures in high-porosity sandstones (this study, Anders and Wiltschko, 1994) suggest that a macroscopic process zone should be expected in high-porosity sandstones.

The tip of the Blueberry Fault, as defined by the point of zero throw, correlates well with the point where through-going slip-surfaces cease to occur. The damage zone at this point is 12 m wide, and deformation band clusters extend for another 45 m ahead of the point of zero throw (Fig. 4). We interpret this as the macroscopic process zone of the Blueberry Fault. The finite width of the damage zone at the point of zero throw is also evident in Fig. 15, which shows that the correlation between damage zone width and throw intercepts the vertical axis at 7 m. The correlation between maximum throw and length for the Chimney Rock Fault array supports this interpretation of a macroscopic process zone. A least squares regression using data from Krantz (1988a) gives a relationship between maximum throw, D, and length, L, of $D = -2.5 + 0.008L$ (with an $R^2 = 0.8$). Because the regression does not pass through the origin it indicates that prior to measurable throw accumulating (i.e. $D > 0$) the length is already of the order of 300 m (i.e. 2.5/0.008). As we have documented, measurable throw only occurs once a through-going slip surface has developed. These observations qualitatively agree with data presented by Fossen and Hesthammer (1997) in their study of displacement-length scaling for deformation bands and faults in high porosity sandstones. Fossen and Hesthammer (1997) showed that there is a change in the scaling exponent (from 0.5 to 1.0) at a fault length of 130–430 m. Furthermore, Fossen and Hesthammer (2000) demonstrate that there is the minimum width to damage zones in a set of cored faults from the Gullfaks Field in porous sandstones, in the northern North Sea. This minimum width is 5–8 m and no slip-surfaces are associated with smaller damage zones. Combining all of these observations we can say that, before there is significant offset, i.e. before a through-going slip surface has formed, we expect to find a zone of deformation band clusters, containing unconnected slip surfaces, that is approximately 5–12 m wide and up to a few hundred metres in length.

8.3. Slip-surface nucleation and development

The model for the growth of deformation bands put forward in Aydin and Johnson (1983) and updated by Antonellini and Aydin (1994) does not focus on the initiation of slip-surfaces, but implies that a certain amount of strain (or number of deformation bands) is required across a zone of deformation bands before a slip-surface nucleates. However, based on our observations, we suggest that slip-surfaces may form at a relatively early stage in the growth of a zone of deformation bands. It appears that slip-surfaces can nucleate in small patches and then propagate and link up to form an anastomosing network of slip-surfaces (Figs. 6–10). This is backed up by the observations of Mair (1997) who found slickenlines on the surface of experimentally generated deformation bands at low values of axial strain (<11%). Aydin and Johnson (1983) and Antonellini and Aydin (1994) did not distinguish if the increased amount of crushing (reduced porosity) around slip-surfaces was a precursor to slip-surface formation or occurred as offset was accumulated. In contrast our porosity results imply that a critical amount of grain crushing or strain is necessary for slip-surface nucleation, and beyond that point slip-surfaces accommodate further strain without an appreciable amount of grain crushing.

Fig. 16 shows the sequential development of faults in high-porosity sandstones that is implied by our results. Initially clusters of deformation bands will form ahead of the fault tip. These clusters may contain short, discontinuous segments of slip surfaces. As the fault continues to propagate, and the strain (or damage zone width) reaches a critical amount, the slip-surfaces coalesce to form a through-going surface allowing the accumulation of a significant amount of offset. As offset is accumulated on the fault surface, deformation band clusters continue to nucleate and grow in the damage zone and new discontinuous slip-surface segments form within the deformation band clusters. The deformation band clusters have an orthorhombic symmetry that is related to a component of along strike extension which is small compared to the across fault extension, and that is not related to the strain field in which the main fault surface is developing. A thin (<30 cm thick) fault core of cataclastic rock develops around the principal slip-surface and discontinuous slip-surfaces anastomose around the main slip-surface. The end result of this process is a principal through-going slip surface that is surrounded by a zone of highly crushed rock (the fault core), and a damage zone consisting of deformation band clusters containing isolated, discontinuous slip-surfaces.

9. Conclusions

Using a combination of field mapping and microstructural analysis we have analysed the variations in throw and damage zone geometry from two faults that developed within a porous sandstone and made the following observations:

1. Within the Navajo Sandstone the damage zone around the Blueberry and Big Hole Faults consists of deformation bands (zones of cataclasis with 7.5–8% porosity) and slip-surfaces that run sub-parallel to the fault. Slip surfaces are thin (<a few mm width) striated surfaces upon which the majority of offset is localised. They are surrounded by very low porosity cataclastic rock (0.5–2.5%). Displacement accumulation on a slip surface has no effect on the grain size (porosity) of the adjacent rock once a slip-surface has initiated. Therefore, microstructural observations alone cannot be used to

distinguish between a minor slip-surface, with only tens of centimetres of throw, and the principal fault plane upon which tens of metres may have accumulated. Short slip-surfaces a few centimetres in length are associated with local thickening of individual deformation bands. Longer slip-surfaces occur in deformation band zones with higher throw and the highest throw slip-surfaces form interconnected networks. The main fault core consists of a zone of concentrated deformation bands with one or more through-going slip-surfaces on one or both sides.

2. The damage zone structures have an orthorhombic geometry with a lower angle between strike sets than the regional fault array. Analysis of this geometry suggests that structures in the damage zone are growing in a local strain field associated with the growth of the main fault rather than the regional strain field. Therefore, the damage zone deformation is due to the displacement accumulation on the main fault and is not a precursor to fault formation. Thus care must be taken when extrapolating from local to regional scale structural geometries.
3. Outside the damage zone few or no deformation bands are seen. The width of the damage zone is positively correlated with the throw on the fault with a slope of 2.5 and an intercept of 7.0 m. Although the predicted damage zone width could vary by as much as 10–20% of the throw, this relationship could be very useful for the prediction of the distribution of sub-seismic deformation around faults in this lithology. Our observations of deformation mechanisms suggest that scaling of damage zone width and throw is likely to be dependent on host rock lithology, in particular high versus low porosity lithologies.
4. The Blueberry Fault can be traced, as a well-developed slip-surface with slickenlines, to its fault tip (zero throw). Beyond the tip, slip-surfaces are discontinuous, confirming that substantial throw cannot have taken place. Deformation bands occur in a zone 12 m wide around the Blueberry Fault tip and continue for 45 m beyond the fault tip. Microfractures within the host rock show no signal associated with the proximity to the fault and we therefore interpret these to be unrelated to the growth of these faults. These observations imply that the process zone in porous sandstones is a macroscopic feature rather than the microscopic process zone described by Anders and Wiltschko (1994) and Vermilye and Scholz (1998) in low porosity rock types. This highlights the difference between the behaviour of high-porosity (>10%) sandstones, and low-porosity sandstones or quartzites.
5. A macroscopic process zone is also consistent with the observation, based on the correlation between throw and length, that faults within the Chimney Rock array do not accumulate measurable throw until they are a few hundred metres in length. Prior to reaching this size, the strain is taken up by a combination of deformation band formation and slip surface nucleation and propagation within a zone up to 15 m wide. This evolutionary process agrees well with the observations of Fossen and Hesthammer (2000) based on displacements and damage zone widths found from well-log correlation and core information.
6. Existing models for the evolution of deformation bands in high porosity sandstones do not describe the details of slip-surface evolution. Our observations show that slip-surfaces nucleate at a relative early stage in the evolution of a zone of deformation bands. As throw is accumulated the slip-surfaces propagate and link within the zone of deformation bands. This distinct microstructural process occurs contemporaneously with the widening of the zone of deformation bands. Until the slip-surfaces link to form a through-going surface, it is not possible for significant throw to accumulate. Because slip surfaces are discrete planes along which significant slip can occur they may represent pathways for fluid flow within a fault zone which otherwise has a very low permeability due to the presence of deformation bands. Therefore, understanding the nucleation, growth and linkage of slip surfaces in three dimensions, and determining whether they are open or closed at depth, will have important implications for understanding the permeability of faults in this lithology.

Acknowledgements

This work benefited greatly from discussions with Jan Vermilye, Bryne Ngwenya, Gerald Roberts and Jim Evans. Haakon Fossen and Ian Davison provided detailed and thoughtful reviews. Iain Main provided useful comments on a first draft of the manuscript. Thanks to Quentin Fisher for assistance collecting the BSEM images. Jon Perry and Ian Martin helped with Erdas Imagine and Optimas. Jan Vermilye, John Mayers, Steve Schulz, Amy Hochberg, Kathryn Hardacre, Richard Jackson, Bertrand Maillot, Clare Bond, Kim Robeson, Jonathan Lim and Steve Thurber assisted with collecting the field data. Z. Shipton was supported by NERC studentship grant GT4/95/91/E with additional help from Bob Krantz (ARCO Alaska). P. Cowie is supported by a University Research Fellowship from the Royal Society of London.

References

Anders, M.A., Wiltschko, D.V., 1994. Microfracturing, palaeostress and the growth of faults. Journal of Structural Geology 16, 795–816.

Antonellini, M.A., Aydin, A., 1994. Effect of faulting on fluid flow in porous sandstones: petrophysical properties. American Association of Petroleum Geologists Bulletin 78, 355–377.

Antonellini, M.A., Aydin, A., 1995. Effect of faulting on fluid flow in porous sandstones: geometry and spatial distribution. American Association of Petroleum Geologists Bulletin 79, 642–671.

Antonellini, M.A., Aydin, A., Pollard, D.D., 1994. Microstructure of

deformation bands in porous sandstones at Arches National Park, Utah. Journal of Structural Geology 16, 941–959.

Antonellini, M.A., Aydin, A., 1999. Outcrop aided characterisation of a faulted hydrocarbon reservoir: Arroyo Grande oil field, California, USA. In: Haneberg W.C., Mozley P.S., Moore, C.J., Goodwin L.B. (Eds.), Faults and Subsurface Fluid Flow, American Geophysical Union Geophysical Monograph 113, 7–26.

Aydin, A., 1978. Small faults formed as deformation bands in sandstone. Pure and Applied Geophysics 116, 913–929.

Aydin, A., Johnson, A.M., 1978. Development of faults as zones of deformation bands and as slip surfaces in sandstones. Pure and Applied Geophysics 116, 931–942.

Aydin, A., Johnson, A.M., 1983. Analysis of faulting in porous sandstones. Journal of Structural Geology 5, 19–31.

Aydin, A., Reches, Z., 1982. Number and orientation of fault sets in the field and in experiments. Geology 10, 107–112.

Beach, A., Brown, J.L., Welbon, A.L., McCallum, J.E., Brockbank, P., Knott, S., 1997. Characteristics of fault zones in sandstones from NW England: application to fault transmissibility. In: Meadows, N.S., Trueblood, S.P., Hardman, M., Cowan, G. (Eds.), Petroleum Geology of the Irish Sea and Adjacent Areas. Geological Society Special Publication 124, 315–324.

Beach, A., Welbon, A.L., Brockbank, P., McCallum, J.E., 1999. Reservoir damage around faults: outcrop examples from the Suez rift. Petroleum Geoscience 5, 109–116.

Brock, W.G., Engelder, T., 1977. Deformation associated with the Muddy Mountain overthrust in the Buffington widow, southeast Nevada. Bulletin of the Geological Association of America 88, 1667–1677.

Caine, J.S., Evans, J.P., Forster, C.B., 1996. Fault zone architecture and permeability structure. Geology 24, 1025–1028.

Cartwright, J.A., Mansfield, C.S., 1998. Lateral displacement variation and lateral tip geometry of normal faults in the Canyonlands National Park, Utah. Journal of Structural Geology 20, 3–19.

Chester, F.M., Logan, J.M., 1986. Composite planar fabric of gouge from the Punchbowl Fault, California. Journal of Structural Geology 9, 621–634.

Chester, F.M., Evans, J.P., Biegel, R.L., 1993. Internal structure and weakening mechanisms of the San Andreas fault. Journal of Geophysical Research 98, 771–786.

Cowie, P.A., Scholz, C.H., 1992. Physical explanation for the displacement-length relationship of faults using a post-yield fracture mechanics model. Journal of Structural Geology 14, 1133–1148.

Cowie, P.A., Shipton, Z.K., 1998. Fault tip displacement gradients and process zone dimensions. Journal of Structural Geology 20, 983–997.

Cox, S.J.D., Scholz, C.H., 1988. On the formation and growth of faults, an experimental study. Journal of Structural Geology 10, 413–430.

Dawers, N.H., Anders, M.A., Scholz, C.H., 1993. Growth of normal faults: displacement-length scaling. Geology 21, 1107–1110.

Dawers, N.H., Anders, M.A., 1995. Displacement-length scaling and fault linkage. Journal of Structural Geology 17, 697–698.

Dunn, D.E., La Fountain, L.J., Jackson, R.E., 1973. Porosity dependence and mechanisms of brittle fracture in sandstones. Journal of Geophysical Research 78, 2403–2417.

Edwards, H.E., Becker, A.D., Howell, J.A., 1993. Compartmentalisation of an aeolian sandstone by structural heterogeneities: Permo-Triassic Hopeman Sandstone, Moray Firth, Scotland. In: North, C.P., Prosser, D.J. (Eds.), Characterisation of Fluvial and Aeolian Reservoirs. Geological Society of London Special Publication 73, 339–365.

Evans, J.P., 1990. Thickness-displacement relationships for fault zones. Journal of Structural Geology 12, 1061–1065.

Fossen, H., Hesthammer, J., 1997. Geometric analysis and scaling relations of deformation bands in porous sandstone. Journal of Structural Geology 19, 1479–1493.

Fossen, H., Hesthammer, J., 2000. Possible absence of small faults in the Gullfaks Field, northern North Sea: implications for downscaling of faults in some porous sandstones. Journal of Structural Geology 22, 851–863.

Fowles, J., Burley, S., 1994. Textural and permeability characteristics of faulted, high porosity sandstones. Marine and Petroleum Geology 11, 608–623.

Foxford K.A., Walsh J.J., Watterson J., Garden I.R., Guscott S.C., Burley S.D., 1998. Structure and content of the Moab fault zone, Utah, USA, and its implications for fault seal prediction. In: Jones, G., Fisher, Q.J., Knipe, R.J. (Eds.), Faulting, Fault Sealing and Fluid Flow in Hydrocarbon Reservoirs. Geological Society Special Publications 147, 71–86.

Hull, J., 1988. Thickness-displacement relationships for deformation zones. Journal of Structural Geology 10, 431–435.

Jamison, W.R., Stearns, D.W., 1982. Tectonic deformation of Wingate sandstone, Colorado National Monument. Bulletin of the American Association of Petroleum Geologists 66, 2584–2608.

Knott, S.D., Beach, A., Brockbank, P.J., Brown, J.L., McCallum, J.E., Welbon, A.I., 1996. Spatial and mechanical controls on normal fault populations. Journal of Structural Geology 18, 359–372.

Krantz, R.W., 1988a. Multiple fault sets and three-dimensional strain: theory and application. Journal of Structural Geology 10, 225–237.

Krantz, R.W., 1988. The odd-axis model: orthorhombic fault patterns and three-dimensional strain fields. PhD Thesis, University of Arizona.

Krantz, R.W., 1989. Orthorhombic fault patterns: the odd-axis model and slip vector orientations. Tectonics 8, 483–495.

Little, T.A., 1996. Faulting-related displacement gradients and strain adjacent to the Awatere strike-slip fault in New Zealand. Journal of Structural Geology 18, 321–342.

Lockner, D.A., Byerlee, J.D., Kuksenko, V., Ponomarev, A., Sidorin, A., 1992. Observations of quasistatic fault growth from aAcoustic emissions. In: Evans, B., Wong, T.F. (Eds.). Fault Mechanics and Transport Properties of Rocks. , pp. 34–67.

McGrath, A.G., Davison, I., 1995. Damage zone geometry around fault tips. Journal of Structural Geology 17, 1011–1024.

Mair, K., 1997. Experimental studies of fault zone development in a porous sandstone. PhD Thesis, University of Edinburgh.

Mair, K., Main, I., Elphick, S., 2000. Sequential growth of deformation bands in the laboratory. Journal of Structural Geology 22, 25–42.

Mansfield, C.S., Cartwright, J.A., 1996. High resolution fault displacement mapping from three-dimensional seismic data: evidence for dip linkage during fault growth. Journal of Structural Geology 18, 249–263.

Martel, S.J., Boger, W.A., 1998. Geometry and mechanics of secondary fracturing around small three-dimensional faults in granitic rock. Journal of Geophysical Research 103, 21299–21314.

Morewood, N.C., Roberts, G.P., 1997. Geometry, kinematics and rates of deformation in a normal fault segment boundary, central Greece. Geophysical Research Letters 24, 3081–3084.

Morewood, N.C., Roberts, G.P., 2000. The geometry, kinematics and rates of deformation in a normal fault segment boundary, central Italy. Journal of Structural Geology 22, 1027–1047.

Muraoka, H., Kamata, H., 1983. Displacement distribution along minor fault traces. Journal of Structural Geology 5, 483–495.

Nicol, A., Walsh, J.J., Watterson, J., Childs, C., 1996. The shapes, major axis orientations and displacement patterns of fault surfaces. Journal of Structural Geology 18, 235–248.

Peacock, D.C.P., Sanderson, D.J., 1996. Effects of propagation rate on displacement variations along faults. Journal of Structural Geology 18, 311–320.

Pittman, E.D., 1981. Effect of fault-related granulation on porosity and permeability of quartz sandstones, Simpson group (Ordovician), Oklahoma. American Association of Petroleum Geologists Bulletin 65, 2381–2387.

Reches, Z., 1978. Analysis of faulting in a three-dimensional strain fields. Tectonophysics 47, 109–129.

Reches, Z., 1983. Faulting of rocks in three-dimensional strain fields II: theoretical analysis. Tectonophysics 95, 133–156.

Roberts, G.P., 1994. Displacement localisation and palaeo-seismicity of the Rencurel Thrust Zone, French Sub-Alpine Chains. Journal of Structural Geology 16, 633–646.

Roberts, G.P., 1996. Variation in fault slip directions along active and

segmented normal fault systems. Journal of Structural Geology 18, 835–845.

Schlische, R.W., Young, S.S., Ackerman, R.V., Gupta, A., 1996. Geometry and scaling relations of a population of very small rift related normal faults. Geology 24, 683–686.

Scholz, C.H., Dawers, N.H., Yu, J.Z., Anders, M.H., 1993. Fault growth and fault scaling laws: preliminary results. Journal of Geophysical Research 98, 21951–21961.

Schulz, S.E., Evans, J.P., 1998. Spatial variability in microscopic deformation and composition of the Punchbowl fault, southern California: implications for mechanisms, fluid-rock interaction and fault morphology. Tectonophysics 295, 223–244.

Shipton, Z.K., 1999. Fault displacement profiles and damage zone geometry: interpreting the record of fault growth in the Navajo Sandstone. PhD Thesis, University of Edinburgh.

Shipton, Z.K., Evans, J.P., Robeson, K., Forster, C.B., Snelgrove, S., 2001. In situ structural and permeability analysis of faulted aeolian sandstone: the Big Hole Fault drilling project, Utah—part 1. American Association of Petroleum Geologists Bulletin (in press).

Vermilye, J.M., Scholz, C.H., 1998. The process zone: a microstructural view. Journal of Geophysical Research 103, 12223–12237.

Walsh, J.J., Watterson, J., 1989. Displacement gradients on fault surfaces. Journal of Structural Geology 11, 307–316.

Witkind, I.J., 1988. Geologic map of the Huntingdon $30' \times 60'$ quadrangle, Carbon, Emery and Uinta counties, Utah.

Wong, T.F., Zhu, W., 1999. Brittle faulting and permeability evolution: hydromechanical measurement, microstructural observation and network modelling. In: Haneberg W.C., Mozley P.S., Moore, C.J.,. Goodwin L.B. (Eds.), Faults and Subsurface Fluid Flow, American Geophysical Union Geophysical Monograph 113, 7–26.

Wong, T.F., David, C., Zhu, W., 1997. The transition from brittle faulting to cataclastic flow in porous sandstones: mechanical definition. Journal of Geophysical Research 102, 3009–3025.

Wu, D., Bruhn, R.L., 1994. Geometry and kinematics of active normal faults, South Orquirrh Mountains, Utah: implication for fault growth. Journal of Structural Geology 16, 1061–1075.